Progress in Oceanography 241 (2026) 103630

Contents lists available at ScienceDirect

Progress in Oceanography

journal homepage: www.elsevier.com/locate/pocean

Zooplankton diel vertical migration and sediment resuspension detected from CEOF analysis of ADCP backscatter in the western Sea of Okhotsk

Kay I. Ohshima [a,b,*], Mamoru Ohshima [c,1], Masato Ito [d], Kazuki Nakata [a,2], Mizuki Kuga [e], Kohei Matsuno [b,f], Atsushi Yamaguchi [b,f]

[a] Institute of Low Temperature Science, Hokkaido University, Sapporo 060-0819, Japan
[b] Arctic Research Center, Hokkaido University, Sapporo 001-0021, Japan
[c] Graduate School of Environmental Science, Hokkaido University, Sapporo 060-0810, Japan
[d] Graduate School of Frontier Sciences, The University of Tokyo, Kashiwa 277-8563, Japan
[e] Fisheries Resources Institute, Japan Fisheries Research and Education Agency, Nagasaki 851-2213, Japan
[f] Faculty of Fisheries Sciences, Hokkaido University, Hakodate 041-8611, Japan

ARTICLE INFO

Keywords:
ADCP
Backscatter strength
Diel vertical migration
Zooplankton
Sediment resuspension
CEOF

ABSTRACT

Acoustic Doppler Current Profilers (ADCPs) provide backscatter strength data, which can be used to detect suspended materials in the water column. This study developed a novel approach to detect and distinguish between zooplankton diel vertical migration (DVM) and sediment resuspension by applying Complex Empirical Orthogonal Function (CEOF) analysis to 24-hour bandpass-filtered ADCP backscatter data. The temporal CEOF mode scores serve as objective scalar indices of the intensity of each phenomenon, enabling quantitative comparisons with environmental factors. We applied this approach to year-round ADCP array observations in the western Sea of Okhotsk. At most sites, DVM activity is represented by the first CEOF mode. Temporal variations of the first mode revealed that, during the sea-ice season, DVM significantly weakens over shelf regions but persists in offshore regions, even though shelf regions exhibit more active biological productivity than offshore regions during the warm season. This contrasting seasonal behavior likely reflects differences in the dominant zooplankton species and their traits. The quantitative assessment of our method revealed clear relationships with tidal currents through spectral analysis. In the northwestern Okhotsk Sea, where tidal currents are strong, DVM activity, represented by the first mode, was consistently reduced during spring tides. At Kashevarov Bank, where tidal currents exceed 1 m/s, the first mode represents sediment resuspension and intensifies ~ 1–1.5 days after peak tidal current velocities, and the second mode captures DVM. Given the vast quantity of unused ADCP backscatter data worldwide, the method proposed here can help unlock the potential of these dormant datasets.

1. Introduction

The Sea of Okhotsk is a marginal sea of the North Pacific and represents the southernmost sea with a sizable seasonal sea ice cover in the Northern Hemisphere. In winter, cold northwesterly winds from the Eurasian continent drive extensive sea ice production along the coastal regions (Nihashi et al., 2009). Sea ice begins to form over the northwestern shelf in late November and is transported southward by the prevailing northwesterly winds and the East Sakhalin Current (ESC) (Simizu et al., 2014). The ice extent reaches its maximum in February–March. Melting and retreat of the sea ice begin in the south in March, and all sea ice in the Sea of Okhotsk melts by the end of June. According to global sea-ice production estimates, the Okhotsk Northwestern polynya exhibits the largest ice production in the Northern Hemisphere (Ohshima et al., 2016).

Until the 1990s, ocean circulation in the Sea of Okhotsk had been described only schematically (e.g., Moroshkin, 1966). Quantitative understanding has been significantly advanced by the joint

* Corresponding author at: Institute of Low Temperature Science, Hokkaido University, Sapporo 060-0819, Japan.
E-mail addresses: ohshima@lowtem.hokudai.ac.jp (K.I. Ohshima), mamoru.ohshima.since96@gmail.com (M. Ohshima), masato-ito@edu.k.u-tokyo.ac.jp (M. Ito), knakata0924@gmail.com (K. Nakata), kuga_mizuki53@fra.go.jp (M. Kuga), k.matsuno@fish.hokudai.ac.jp (K. Matsuno), a-yama@fish.hokudai.ac.jp (A. Yamaguchi).
[1] Tokyo Electric Power Company, Incorporated, Kashiwazaki 945-8601, Japan (current affiliation).
[2] Earth Observation Research Center, Japan Aerospace Exploration Agency, Tsukuba 305-8505, Japan (current affiliation).

https://doi.org/10.1016/j.pocean.2025.103630
Received 19 July 2025; Received in revised form 5 October 2025; Accepted 21 November 2025
Available online 26 November 2025

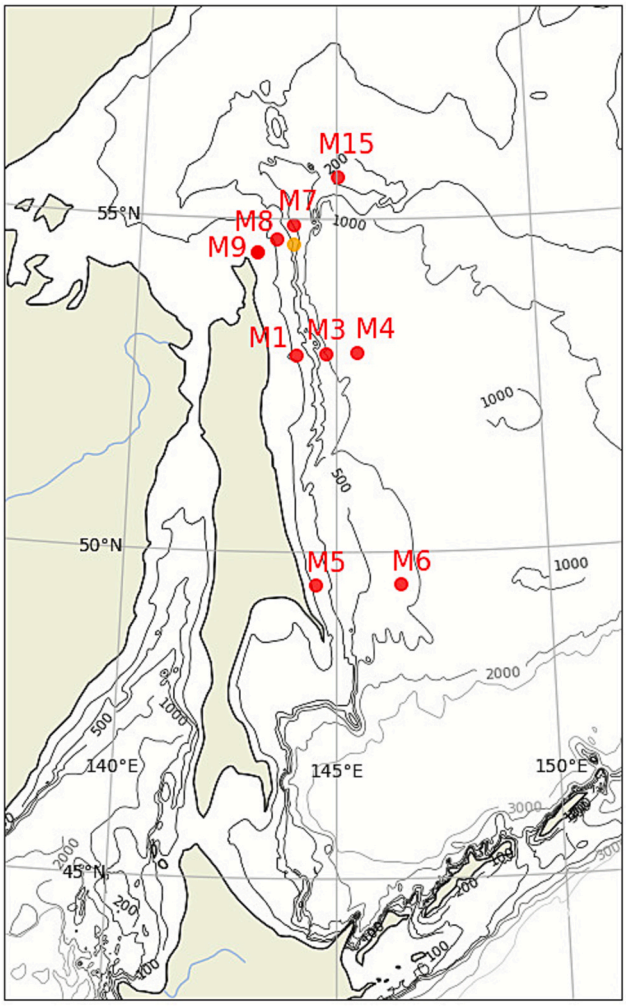

Fig. 1. Bathymetry of the study area based on the General Bathymetric Chart of the Oceans (GEBCO) data, showing locations of the ADCP observations (red solid circles). Observations at M1, M3, M5, and M6 were conducted from July 1998 to September 1999, and at M4, M6, M7, M8, M9, and M15 from September 1999 to June 2000. For mooring M7, which was displaced by strong currents, red and orange circles denote the deployment and recovery locations, respectively. Bathymetric contours of 100, 200, 500, 1000, 2000, and 3000 m are indicated by solid lines.

Japanese–Russian–U.S. study of the Sea of Okhotsk. In the central and northern parts of the sea, a cyclonic gyre dominates, with a strong southward flow of the ESC along the Sakhalin Island coast (Mizuta et al., 2003). The ESC consists of two branches: a nearshore branch and an offshore branch (Ohshima et al., 2002). Both branches exhibit strong seasonal variations, with maximum transport in winter and minimum transport in summer (Mizuta et al., 2003; Simizu and Ohshima, 2006).

Seasonal sea ice zones, such as the Sea of Okhotsk, generally provide rich biological resources, mainly originating from extensive phytoplankton blooms associated with sea-ice melt (hereafter referred to as the spring bloom). The increased vertical stability from freshwater supplied by sea-ice melt enhances light availability, providing favorable conditions for phytoplankton growth (Niebauer et al., 1990; Sorokin and Sorokin, 1999), in addition to the enhanced nutrient supply provided by convective mixing during the preceding winter. Moreover, micronutrients such as iron released from sea ice and ice algae are considered to contribute to the prominent spring bloom (Kanna et al., 2014; 2018; Yan et al., 2020). The relationship between sea-ice melt and the spring bloom has also been suggested by satellite observations in the Sea of Okhotsk (Nihashi et al., 2012). Kishi et al. (2021) showed that the prominent spring bloom in the southern Sea of Okhotsk is strongly linked to sea-ice melt, based on net community production estimated from profiling float oxygen data.

With regard to biological resources, mesozooplankton are of prime importance. A comprehensive review of zooplankton in the Sea of Okhotsk was provided by Pinchuk and Paul (2000). Concerning diel vertical migration (DVM) of zooplankton in the Sea of Okhotsk, Pinchuk and Paul (2000) introduced early studies by Vinogradov (1954), who listed copepods such as *Metridia* spp. (*M. okhotensis* and *M. pacifica*), and euphausiids as species exhibiting strong DVM. The vertical distribution of zooplankton was also investigated through net sampling during the aforementioned joint Japanese–Russian–U.S. study of the Sea of Okhotsk (Itoh et al., 2014; Tsuda et al., 2015), which revealed geographic variability in the vertical distribution of dominant species, especially copepods, However, because sampling at each station was conducted only once, these studies could not assess DVM or its geographic variability. Yamaguchi (2015) and Arima et al. (2016) showed that *M. okhotensis* dominates the copepod community as major zooplankton abundance in the Sea of Okhotsk. Although there has been a series of investigations on zooplankton in the Sea of Okhotsk, the interaction between sea ice and zooplankton dynamics remains poorly understood.

It has been shown, through both numerical model simulations (Kowalik and Polyakov, 1998; Nakamura et al., 2000; Ono and Ohshima, 2010) and observational studies (Rabinovich and Zhukov 1984; Ohshima et al. 2002), that the Sea of Okhotsk is characterized by strong diurnal tidal currents. This is partly because the natural oscillation period in the region is close to diurnal periods (Kowalik and Polyakov, 1998). Additionally, the high-latitude location of the Sea of Okhotsk permits the existence of topographic Rossby waves at diurnal periods. Amplification of diurnal tidal currents over the northern Sakhalin shelf can be explained by diurnal coastal-trapped waves (CTWs) (Ono et al. 2008), and particularly strong amplification over Kashevarov Bank (Fig. 1) arises from resonance with seamount-trapped

Table 1
Summary of ADCP observation details: location, bottom depth, nominal depth, time interval, bin size, instrument type, and observation period.

Station	Lattitude	Longitude	Water depth	Nominal depth	Time interval	Bin size	ADCP type	Period
	(°N)	(°E)	(m)	(m)		(m)		
M1	53.0	144.0	100	100	1 h	4	Workhorse	1998/07/27–1999/07/11
M3	53.0	144.8	970	190	1 h	8	BroadBand	1998/07/28–1999/09/07
M4	53.0	145.5	1720	180	1 h	8	BroadBand	1999/09/06–2000/06/17
M5	49.5	144.5	130	130	1 h	4	Workhorse	1998/08/01–1999/07/15
M6	49.5	146.5	790	180	1 h	8	BroadBand	1998/08/02–1999/09/04
M6	49.5	146.5	790	180	1 h	8	BroadBand	1999/09/24–2000/06/15
M7	54.9	143.9	480	200	1 h	8	BroadBand	1999/09/10–1999/12/09
M7			440	160	1 h	8	BroadBand	1999/12/10–2000/03/19
M7	54.6	143.9	620	340	1 h	8	BroadBand	1999/03/20–2000/06/27
M8	54.7	143.5	110	110	30 min.	4	Workhorse	1999/12/12–2000/03/24
M9	54.5	143.0	90	90	15 min.	4	Workhorse	1999/09/19–2000/03/16
M15	55.6	145.0	138	138	1 h	4	Workhorse	1999/09/20–2000/06/20

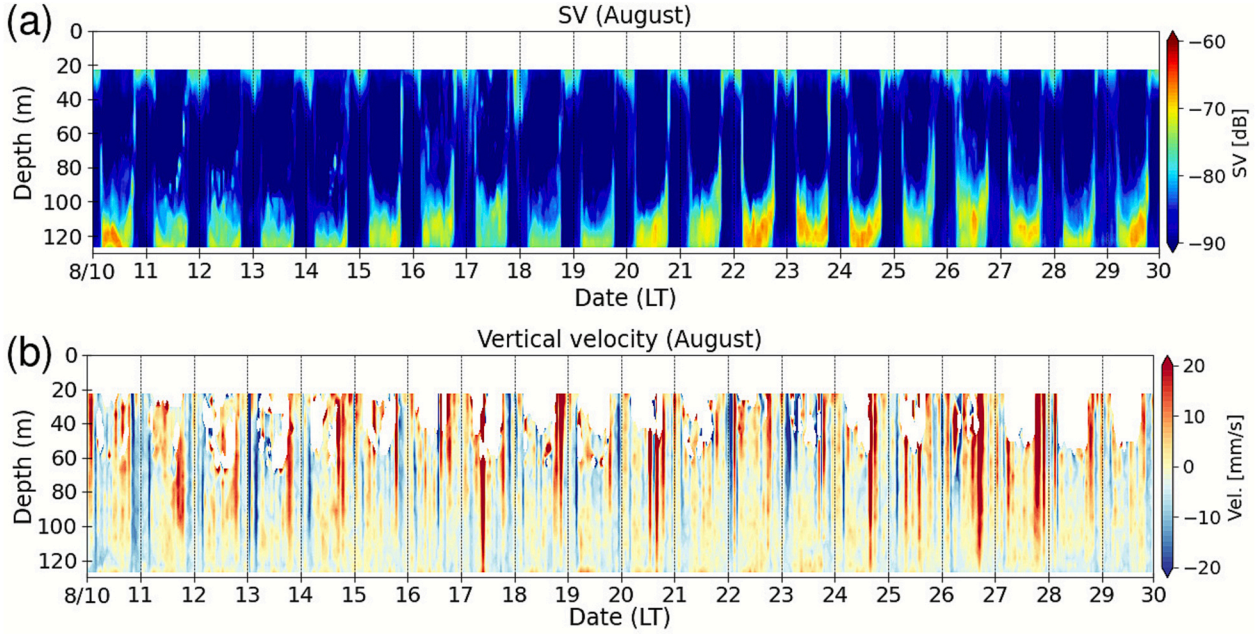

Fig. 2. Time series of vertical profiles of (a) original ADCP volume backscatter strength (SV) and (b) vertical velocity (positive upward) from the ADCP at M5 from 10 to 29 August 1998. Ticks on the horizontal axis correspond to 00:00 (local time: UTC + 9h).

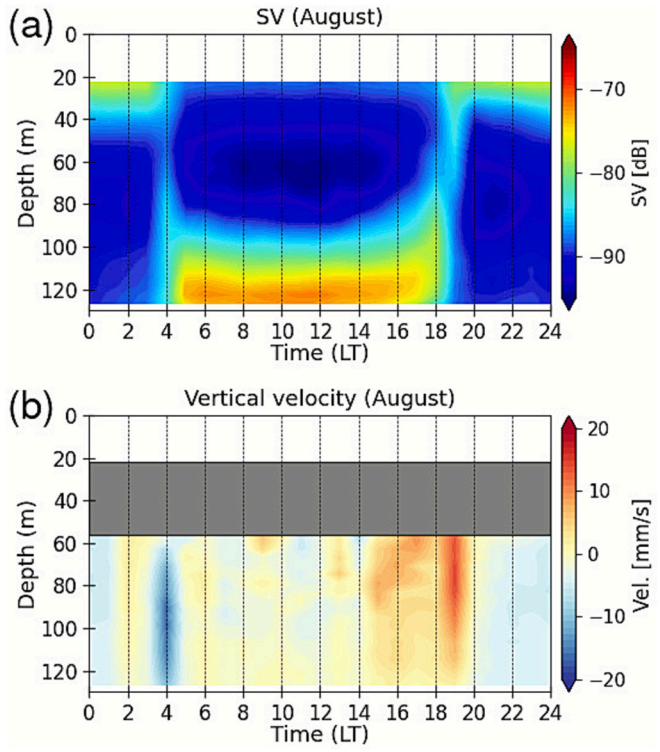

Fig. 3. Vertical profiles of 24-hour composites of (a) ADCP volume backscatter strength (SV) and (b) vertical velocity at M5 over the 31 days of August 1998. Ticks on the horizontal axis correspond to the top of the hour (local time). Since the vertical velocity distant from the ADCP contains large errors, layers with the distance of > 70 m from the ADCP are masked.

waves (Ono et al., 2006). These strong tidal currents likely influence ocean circulation, water mass transformation, sea ice processes, material transport, and biological activity (Rogachev et al., 2001; Martin et al., 2004).

Mooring-based ADCP observations have revealed both circulation and tidal variability in the Sea of Okhotsk. In addition to velocity profile, ADCPs also provide volume backscatter strength data, which can detect suspended particles in the water column. In this region, signals associated with underwater frazil ice (Ito et al., 2017, 2020, 2021), sediment resuspension (Ito et al., 2017), and DVM of zooplankton have been reported. Among these, DVM appears to be the dominant backscatter signal at most mooring sites, as will be shown. Nevertheless, no studies have yet analyzed DVM using ADCP data in the Sea of Okhotsk. Although backscatter signatures from frazil ice, sediment resuspension, and DVM are often recognizable, few robust methodologies exist for distinguishing among these signals. In particular, it is challenging to distinguish between DVM, which has a diurnal cycle, and sediment resuspension, which also exhibits a diurnal cycle due to tidal currents. Furthermore, no objective indicator has been proposed to quantify the intensity of these processes.

In this study, we apply complex empirical orthogonal function (CEOF) analysis as a method to distinguish between DVM and sediment resuspension and to quantify their respective intensities. Section 2 outlines the data and observations followed by derivation of the volume backscatter strength from the ADCP data. Section 3 presents the application of CEOF analysis to the time series data of vertical profiles of the backscatter strength, using two sites as examples. In particular, we demonstrate the effectiveness of the CEOF analysis to discriminate between DVM and sediment resuspension for one site. Section 4 applies the method to the ADCP array data set in the ESC region to elucidate the spatial and seasonal variability of DVM with its relationship to sea ice and chlorophyll concentration. Section 5 applies the CEOF analysis to ADCP data acquired over the northern Sakhalin shelf to investigate the DVM variation with its relationship to tidal currents.

In other sea-ice-covered oceans, such as the Arctic Ocean, there have been a series of studies on DVM in relation to sea ice using ADCP backscatter (Berge et al., 2015; Cohen et al., 2015; Petrusevich et al., 2016; 2020; Dmitrenko et al., 2020; 2024; Flores et al., 2023). Petrusevich et al. (2020) applied wavelet analysis to ADCP-derived horizontal and vertical velocities to examine the relationship between zooplankton DVM and spring–neap as well as seasonal variability in Hudson Bay, a seasonally ice-covered region. The present study likewise focuses on the relationship between DVM and sea ice.

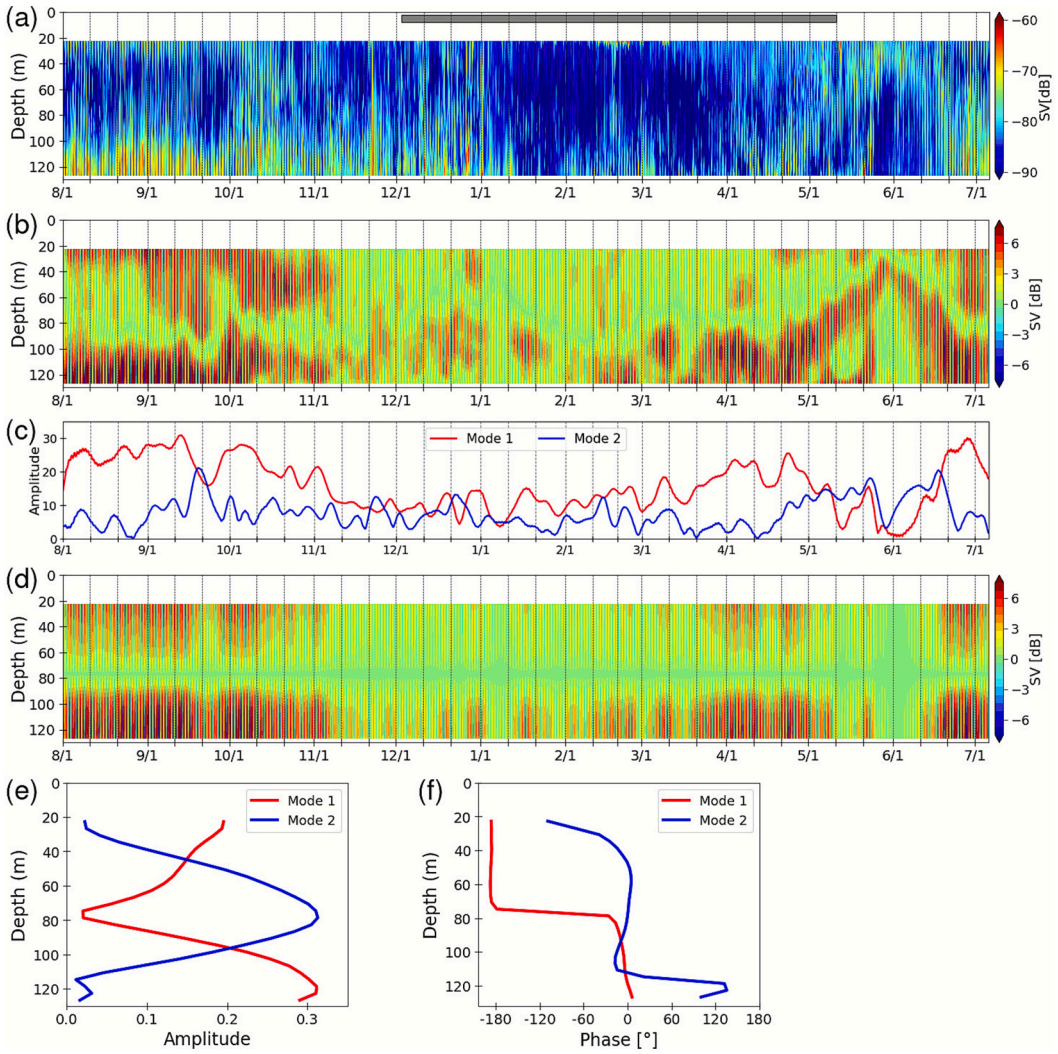

Fig. 4. Time series of vertical profiles at M5 of (a) original ADCP volume backscatter strength (SV), (b) 24-hour bandpass-filtered SV, (c) scores of the first (red) and second (blue) CEOF modes, and (d) reconstructed first CEOF mode, over the entire observation period. (e) Spatial amplitudes and (f) spatial phases of the first and second CEOF modes. The gray bar in (a) indicates the sea-ice-covered period (ice concentration > 15 %).

2. Observation and data

The ADCP observations were conducted between 1998 and 2000 as part of the joint Japanese–Russian–U.S. study of the Sea of Okhotsk. Deployment locations are shown in Fig. 1. Two ADCPs were deployed along 49.58°N (M5, M6), three along 53.8°N east of Sakhalin Island (M1, M3, M4), three along a northeastward line from the northern tip of Sakhalin Island (M7, M8, M9), and one over Kashevarov Bank (M15), a shallow submarine bank on the northern continental slope. Sites M1, M5, M8, M9, and M15 were located on the continental shelf, where upward-looking 300-kHz ADCPs (RD Instruments Workhorse Sentinel) were mounted on the seafloor, enabling full water-column profiling. These instruments were installed using trawl-resistant bottom mounts (TRBM; Flotation Technologies AL-200) to protect against fishing activity. Sites M3, M6, and M7 were located on the slope, and site M4 was located in the deep offshore basin; at these sites, upward-looking 150-kHz ADCPs (RD Instruments Broadband) were moored, allowing profiling of the upper ~ 200 m. Mooring M7 was displaced by strong currents and recovered approximately 29 km downstream from its original deployment site (Fig. 1). The depth data from the ADCP showed two significant shifts during the observation period. The estimated bottom depths at M7 were approximately 480 m (September–November), 440 m (December–March), and 620 m (March–June).

Details of the ADCP observations are summarized in Table 1. Data were recorded at intervals ranging from 15 min to one hour. For analysis, we assumed that the instruments remained at the nominal depths listed in Table 1 throughout the observation periods. The acoustic cell length was set to either 4 m or 8 m. We calculated the volume backscatter strength, SV, from the acoustic backscatter strength (echo amplitude) data obtained by the ADCPs, following the sonar equation of Deines (1999) and the near-field correction of Downing et al. (1995).

SV, defined as the target strength per unit volume, is expressed as:

$$SV = 10 \log_{10} \sigma,$$

where σ is the net backscatter cross-section per unit volume. The detailed calculation procedure follows Ito et al. (2017; 2021). The ADCP frequencies used in this study (300 kHz and 150 kHz) correspond to wavelengths of approximately 5 mm and 10 mm, respectively. These wavelengths are suitable for detecting copepods with body lengths of about 1–5 mm and krill with body lengths of about 1–10 mm.

We used daily sea-ice concentration data derived from the Special Sensor Microwave Imager (SSM/I) to assess sea-ice conditions near the ADCP sites. Ice concentration was calculated using the bootstrap algorithm (Comiso et al., 1995) at a spatial resolution of 25 km. We used chlorophyll-a concentration data obtained from the SeaWiFS sensor onboard the OrbView-2 satellite, which is equipped with eight spectral

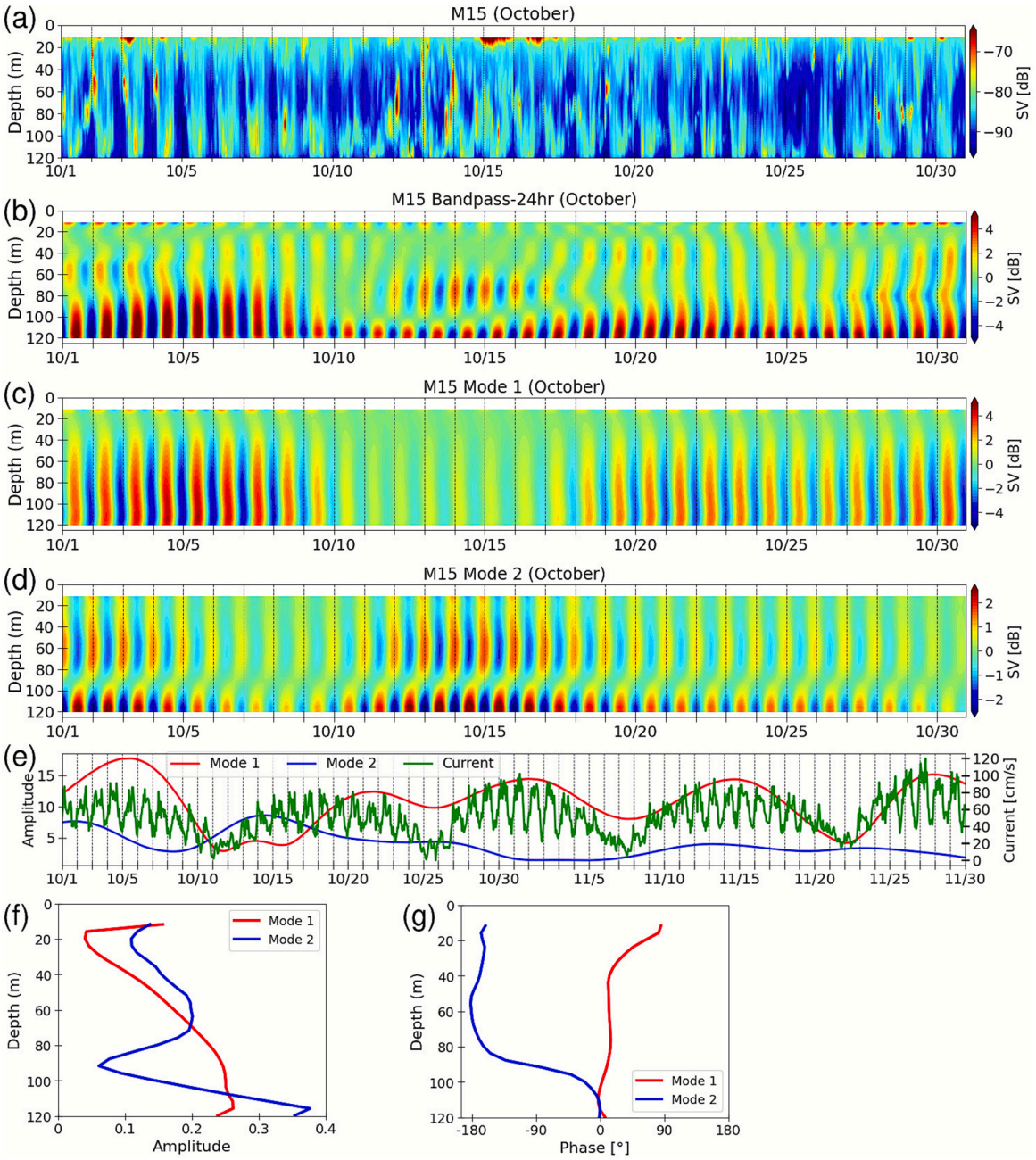

Fig. 5. Time series at M15 from 1 to 30 October 1998 of (a) original ADCP volume backscatter strength (SV), (b) 24-hour bandpass-filtered SV, (c) reconstructed first CEOF mode, (d) reconstructed second CEOF mode. (e) Time series of scores of the first (red) and second (blue) CEOF modes with the current speed at the deepest bin (green) at M15 during October–November 1998. (f) Spatial amplitudes and (g) spatial phases of the first and second CEOF modes. The CEOF calculation is based on the entire ~ 10-month time series.

bands (412–865 nm). These data were provided by NASA's Ocean Biology Processing Group.

3. CEOF analysis with bandpass filtering

In this section, we explain the methodology and effectiveness of CEOF analysis using two example sites: M5, where only the diurnal cycle of DVM dominates, and M15, where both DVM and diurnal sediment resuspension are prominent. As an example of the time series of vertical profiles of SV (volume backscatter strength) when DVM clearly appears, we present the August data for M5 (Fig. 2a). M5 is located on the continental shelf at a depth of 130 m, where an ADCP was installed on the seafloor, allowing full-depth profile acquisition.

Fig. 2a shows that strong signals rise to the near-surface layer toward nighttime and descend to deeper layers toward the daytime. This pattern indicates that the backscatter arises from the diurnal vertical migration (DVM) of zooplankton. Fig. 2b shows the corresponding time series of vertical velocity from the ADCP. The observation at M5 used a trawl-resistant bottom mount (TRBM), ensuring the ADCP remained fixed and allowing relatively reliable vertical velocity measurements. When compared with the SV data (Fig. 2a), downward velocity frequently occurs in the morning as strong SV signals move downward, while upward velocity is observed in the evening as SV signals rise. These velocities typically range from 15 to 20 mm/s (54 to 72 m/h) and are interpreted as the swimming speeds of suspended zooplankton rather than water velocities. The DVM observed here is likely caused by

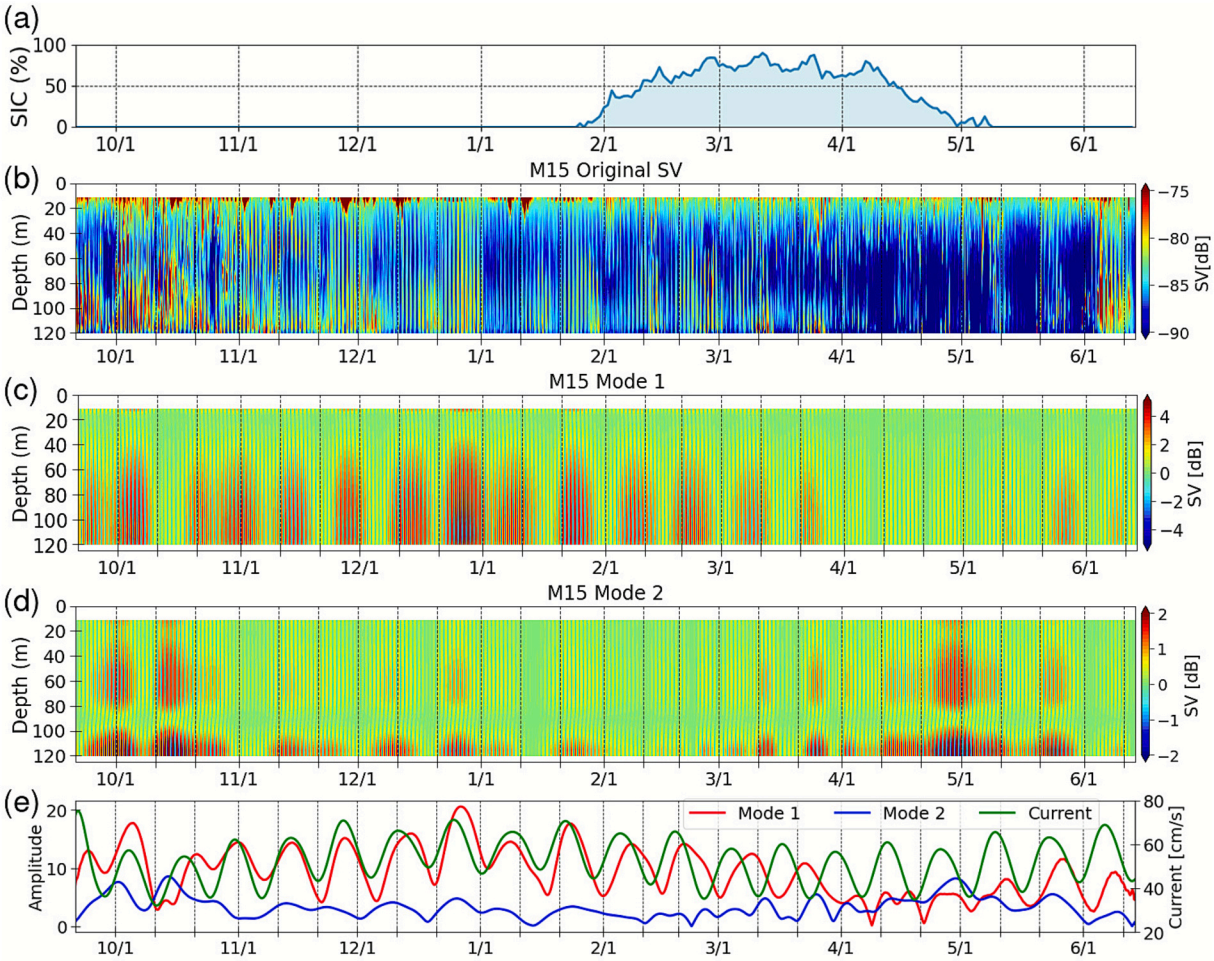

Fig. 6. Time series at M15 over the entire ~ 10-month observation period of (a) sea ice concentration, (b) original ADCP volume backscatter strength (SV), (c) reconstructed first CEOF mode, and (d) reconstructed second CEOF mode. (e) Time series of the scores of the first (red) and second (blue) CEOF modes and the absolute velocity with a fortnightly bandpass filter at the near-bottom bin (green).

copepods (Vinogradov, 1954; Kojima et al., 2022), and the swimming speeds roughly align with previous reports, which range from 8 to 25 mm/s (29 to 90 m/h) for *M. pacifica* (Enright, 1977; Wong, 1988; Mauchline, 1998).

Fig. 3 shows a 24-hour composite of the vertical profiles of SV and vertical velocity over the 31 days of August. For SV (Fig. 3a), a clear DVM pattern is evident: during daylight hours (04:00 to 19:00), strong signals appear from the seafloor up to 20 m, while at night, strong signals are confined to shallower than 30 m. For vertical velocity (Fig. 3b), downward and upward flows correspond to the downward and upward movements of SV signals, respectively. As the velocities are averaged, the composite velocities tend to be smaller than the instantaneous velocities in Fig. 2b, typically around 10–15 mm/s (36–54 m/h). Taken together with the raw vertical velocity data shown in Fig. 2b, these results demonstrate that the swimming speed of zooplankton can be measured using ADCP.

To extract a spatially consistent structure, such as DVM, from the vertical profile time series, CEOF analysis offers distinct advantages, compared with other methods such as wavelet analysis. First, CEOF simultaneously extracts temporal amplitude and phase variability, allowing coherent representation of a vertically propagating signal such as DVM. Wavelet analysis is primarily designed for time–frequency localization and is less effective in isolating such spatially consistent structures. Second, CEOF decomposes the dataset into dominant variability modes and quantifies their relative contributions.

In this study, we propose a method combining bandpass filtering and CEOF analysis to extract the DVM component and represent its intensity as a time series. Specifically, the method first applies a strong bandpass filter with a center frequency of 24 h to the original SV data, and then the CEOF analysis is performed. As will be demonstrated later, in regions with strong tidal currents, this method may also capture sediment resuspension events; however, due to differences in phase, they are clearly distinguishable from DVM. In this study, we apply this method to ADCP data obtained in the western part of the Sea of Okhotsk to quantify zooplankton DVM and analyze its relationship with environmental factors such as tidal currents and sea ice.

Fig. 4 illustrates the application of this method to year-round SV data at M5. First, we applied a bandpass filter with cutoff periods of 23 and 25 h using the Hamming window function from Python's SciPy library to isolate diurnal signals. Next, we performed CEOF analysis on the bandpass-filtered SV time series of Fig. 4b. The necessary Hilbert transformation and eigenvalue calculations were conducted also using Python's SciPy library. Specific procedure of CEOF analysis is briefly described in Appendix, and an example of Python code for the CEOF analysis of SV vertical profile timeseries is provided in the Supplementary material. The CEOF analysis showed that the first, second, and third modes account for 72 %, 18 %, and 5 % of the variability, respectively, indicating that the first mode explains most of the variability. Figs. 4e and 4f present the spatial amplitude and phase of the first/second CEOF modes, respectively. The spatial amplitude of the first mode peaks near the surface at nighttime and near the seafloor during the daytime, with an approximate 180-degree phase difference, clearly reflecting the DVM

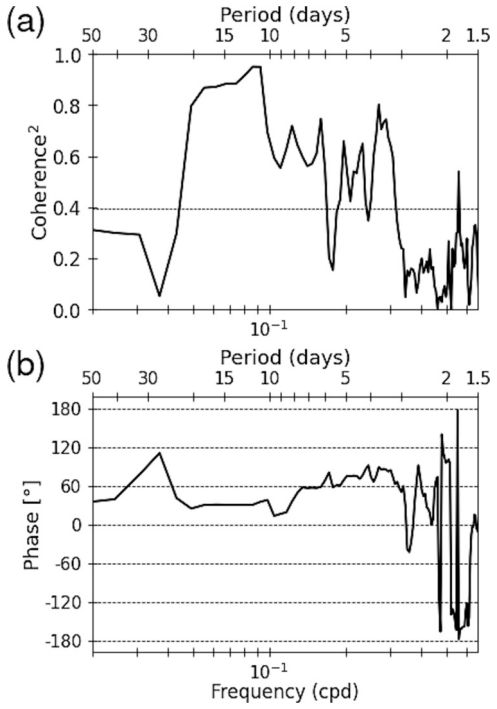

Fig. 7. (a) Squared coherence and (b) phase of the cross-spectra between the first CEOF mode and near-bottom current speed at M15 for the period from September to February. A positive phase indicates that the first CEOF mode leads the bottom current. The 95% confidence level is shown in (a).

pattern. Fig. 4c shows the time series of the first and second mode scores over the entire data period (approximately one year). The weakening of DVM activity during the sea ice season (December to March) is quantitatively captured in the first mode score. To visually represent the DVM activity quantified by the first mode along with the phase information, the time series of the reconstructed first CEOF mode is shown (Fig. 4d). For subsequent analyses, we will use this reconstructed CEOF mode to better visualize DVM behavior.

We next present the analysis of M15 as an example where both DVM and sediment resuspension occur simultaneously. M15 is located on Kashevarova Bank, where strong diurnal tidal currents of up to 2.0 m/s are generated due to excitation of sea-mount trapped waves (Ohshima et al., 2002; Ono et al., 2006). Fig. 5a is the time series of the original SV for October at M15, displaying a clear diurnal signal. However, unlike M5 in Fig. 2, the vertical phase difference of SV is small, and the signal appears to fluctuate nearly in phase across depths.

We applied a bandpass filter with cutoff periods of 22 and 26 h and CEOF analysis to approximately 10 months of SV data at M15. The CEOF results show that the first, second, and third modes account for 81 %, 11 %, and 4 % of the variability, respectively, indicating that over 90 % is captured by the first two modes. The October portion of the CEOF results is shown in Fig. 5, including the time series of the bandpass-filtered data (Fig. 5b) and reconstructed first and second modes (Figs. 5c and 5d).

Fig. 5e shows the October–November time series of the first and second mode scores, along with the absolute current velocity at the near-bottom bin of the ADCP. Figs. 5f and 5g present the spatial amplitude and spatial phase of the first/second CEOF modes, respectively. The first mode exhibits little vertical phase difference and stronger amplitude near the seafloor. Fig. 5e demonstrates that the amplitude of the first mode becomes large during spring tides or shortly afterward, while it becomes small during neap tides. In the shelf area (M8 and M9) adjacent to the bank, Ito et al. (2017) showed that sediment suspension and dispersion occurred during periods of strong current of around 1.0 m/s, from the ADCP backscatter, and rationalized its occurrence by calculating the critical shear stress for sediment resuspension, based on the particle size reported by Sakamoto et al. (2005). If we assume that sediment particle size at M15 is similar to that at M8 and M9, sediment suspension and dispersion would occur during spring tides at M15, when near-bottom current velocities reach around 1.0 m/s (Fig. 5e). All these considered, the first CEOF mode represents sediment resuspension induced by strong bottom currents. On the other hand, the second mode shows a phase difference of approximately 180 degrees between depths shallower than 80 m and the near-seafloor (Fig. 5g). The amplitude becomes its maximum near the seafloor during the daytime (Fig. 5f). Based on these amplitude and phase characteristics, the second mode is considered to represent zooplankton DVM.

Fig. 6 presents the time series of the original SV and the results of CEOF analysis at M15 over the entire 10-month observation period. Fig. 6e shows the first and second mode scores and near-bottom current speed with a bandpass filter centered at fortnightly periods. The first mode score exhibits a clear relationship with the 14/15-day spring-neap tidal cycle observed in the currents. The first mode score increases when tidal currents strengthen or shortly afterward and decreases when tidal currents weaken. On the other hand, the second mode score, which represents DVM, becomes small during the sea-ice period (December to March), similar to the case of M5, and increases during the ice-melt period and immediately afterward (April–May), reaching a magnitude comparable to the first mode. These characteristics remain consistent when the same CEOF analysis is performed on a monthly basis. The CEOF analysis not only allows for the clear separation of sediment resuspension and DVM but also enables the quantification of their intensities as time series of the first and second mode scores, facilitating various time series analyses.

As a specific example, Fig. 7 shows the cross-spectrum between the first mode score and the absolute current velocity to quantify the relationship between sediment resuspension and current velocity, where we calculated the cross-spectrum for the period from September to February, when the first mode dominated. The results showing very high coherence at fortnightly periods statistically confirm a strong relationship between sediment resuspension and tidal currents. A phase lag of ~ 30 degrees indicates that sediment resuspension (CEOF mode 1) reaches its peak about 1–1.5 days after the peak in tidal currents. As seen in Fig. 6e, this lag may vary seasonally. However, it remains unclear whether these phase relationships are statistically significant, and even if they are, the underlying physical mechanisms are still uncertain.

4. Application to the region of the east Sakhalin current

In this section, we apply the CEOF-based method developed in this study to the ADCP data widely obtained off the east Sakhalin coast. Before showing the results of the CEOF analysis, we present the year-long time series of original SV data at observation sites in the East Sakhalin Current region and offshore (M1, M3, M4, M5, M6) (Fig. 8). M1, M3, and M4 were located at 53°N, while M5 and M6 were located at 49.5°N (Fig. 1), allowing for north–south comparisons. Additionally, comparisons can be drawn between different regions: coastal sites (M1: bottom depth 100 m; M5: bottom depth 130 m), continental slope sites (M3: 970 m; M6: 790 m), and the basin site (M4: 1720 m). Notably, SV sensitivity depends on the individual ADCP instruments, implying that absolute SV intensities cannot be directly compared across sites; however, seasonal variations and depth-dependent differences within each site can still be effectively analyzed.

In Fig. 8, the strong signals observed are mostly attributed to DVM activity, which fluctuates on a daily cycle. A notable and consistent feature across all sites is the sharp increase in backscatter strength immediately after sea-ice melt. This is likely due to the spring bloom triggered by enhanced stratification and the release of micronutrients such as iron upon ice melt (Kanna, 2014; 2018; Kishi et al., 2021), which promotes the rapid growth of zooplankton feeding on phytoplankton.

Another common feature is that during the sea-ice season (indicated

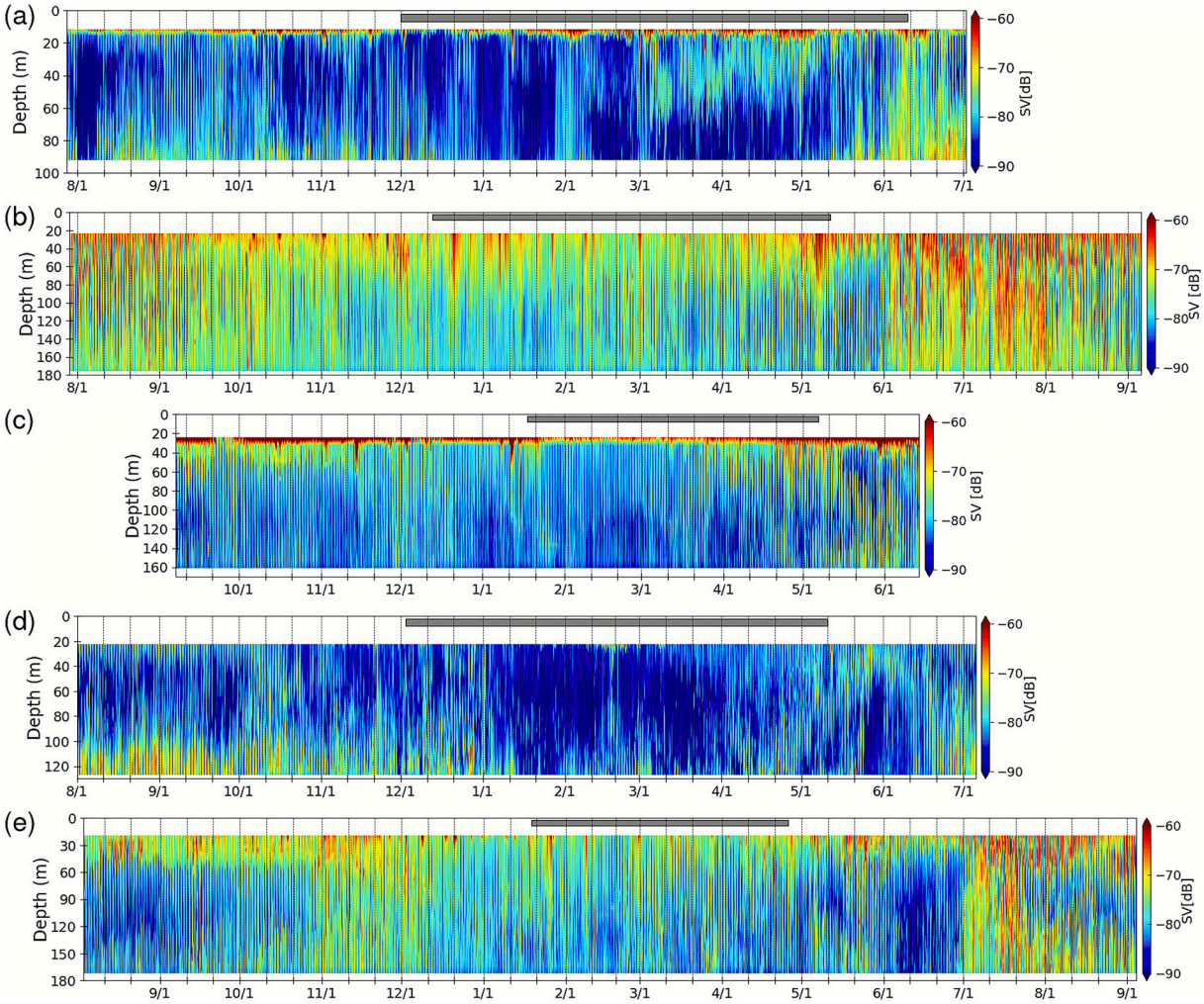

Fig. 8. Time series of vertical profiles of original volume backscatter strength (SV) off the east Sakhalin coast at (a) M1, (b) M3, (c) M4, (d) M5, and (e) M6. Observations were conducted from July 1998 to September 1999 for M1, M3, M5, and M6, and from September 1999 to June 2000 for M4. The gray bar at the top of each panel indicates the sea-ice-covered period (ice concentration > 15 %).

by gray bars in Fig. 8), the backscatter strength tends to decrease, or relatively strong signals are confined to the near-surface layers. This is because, in addition to the inherently weak solar radiation during this period, the presence of sea ice further reduces the penetration of sunlight into the water column and weakens the diurnal cycle of light variation. As a result, DVM behavior, which serves to avoid visual predation, becomes weaker, and the migration depth becomes shallower (Takahashi et al., 2009). The seasonality of DVM and its regional differences can be quantitatively assessed through the CEOF analysis presented below.

Here, we present the results of the CEOF analysis for all sites off the east Sakhalin coast. As in Fig. 4, we conducted the CEOF analysis with a 24-hour bandpass filtering for the entire time series of SV at each site. At all sites, the first CEOF mode consistently exhibits a pattern of large amplitude near the surface at night and large amplitude near the seafloor or in the lower layer during the daytime, as seen in Fig. 4 for M5, representing DVM. The contribution of the first mode at M1, M3, M4, M5, and M6 is 63 %, 82 %, 94 %, 72 %, and 81 %, respectively, indicating that at all sites, the first mode representing DVM accounts for most of the variability.

Accordingly, Fig. 9 presents the time series of the reconstructed first CEOF mode at all sites off the east Sakhalin coast. providing a clear visual representation of both the vertical structure and temporal changes in amplitude. Time series of sea-ice concentration at each site are also shown in Fig. 9. Note that only M4 data correspond to the 1999/2000 season, while the other sites are from the 1998/1999 season (Table 1). In both the M1–M3/M4 and M5–M6 pairs, coastal sites exhibit a marked weakening of DVM during sea-ice season, whereas offshore sites exhibit continued DVM activity even in sea-ice season. When comparing the reconstructed first mode at the shelf sites M1 and M5, DVM activity recovers from April at the southern site (M5) as sea-ice reduction and melt progress, whereas DVM recovers from early June at the northern site (M1), corresponding to the delayed sea-ice reduction and melt.

Satellite-observed chlorophyll-a concentrations (Fig. 10) show that the spring bloom has not yet started at the northern M1 site in May, while the southern M5 site already exhibits high chlorophyll-a levels, indicating active blooming. These results suggest that blooming associated with sea-ice melt and the subsequent activation of zooplankton occur progressively from the southern to the northern regions, following the shift in the sea-ice melt season.

At the shelf sites (M1 and M5), bottom-mounted ADCPs enabled full water-column observations. The first CEOF mode exhibited a structure characterized by large amplitudes near the seafloor during the daytime and near the surface at night, with a 180-degree phase difference between upper and lower layers. This pattern likely represents DVM by copepods (Pinchuk and Paul, 2000). In the shelf regions, the first mode amplitude and thus DVM activity becomes weak during the winter sea-ice season. In contrast, at the slope sites (M3 and M6) and the basin site

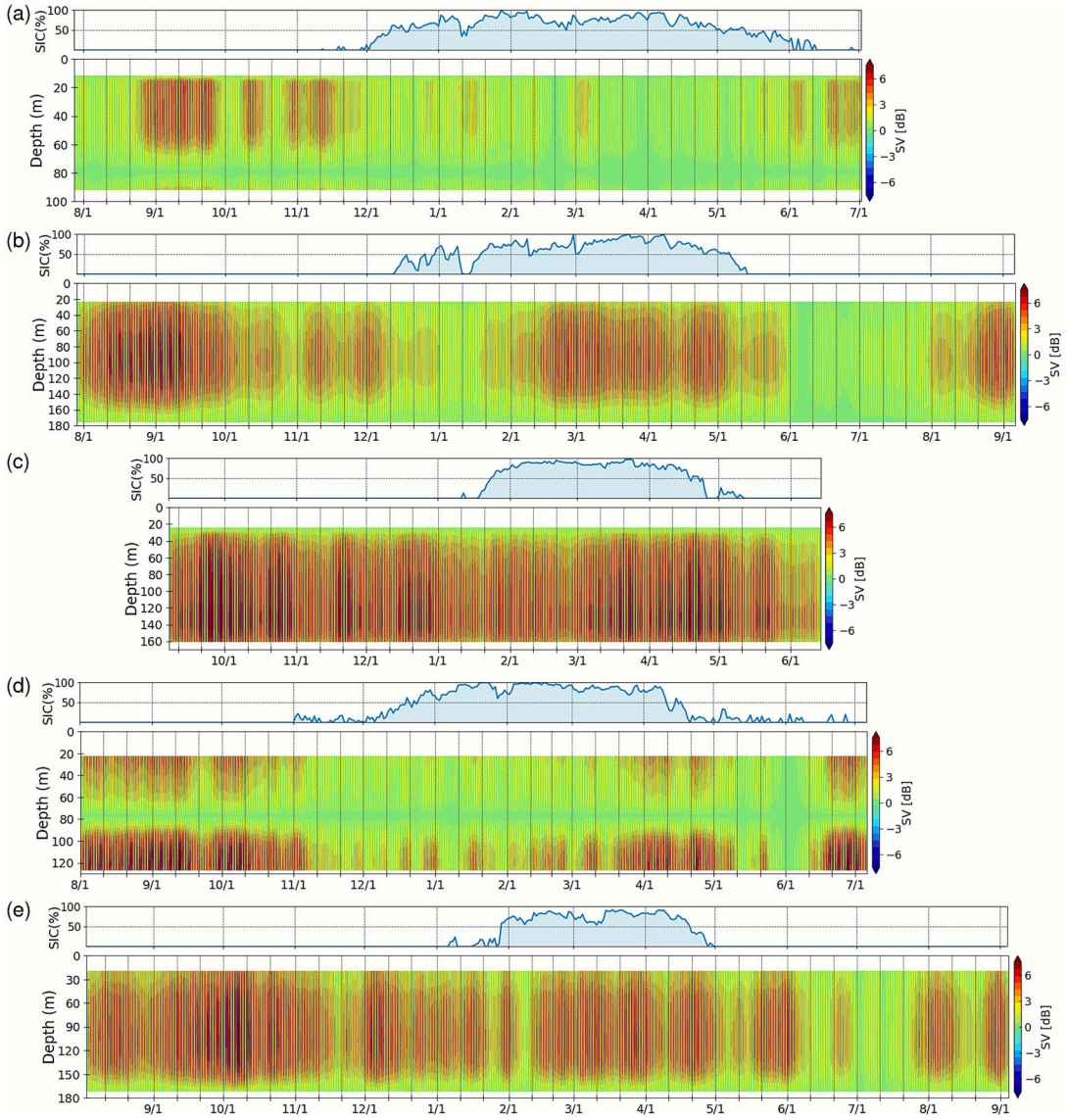

Fig. 9. Time series of (upper panels) sea ice concentration and (lower panels) reconstructed first CEOF mode vertical profiles off the east Sakhalin coast at (a) M1, (b) M3, (c) M4, (d) M5, and (e) M6. The SSM/I ice concentration at the grid point closest to the observation site is shown.

(M4), the first mode, unlike at M1 and M5, maintained similar amplitudes even during the winter sea-ice season, suggesting that DVM activity is not weakened by sea ice in these regions. The ADCP installation depths were ~ 190 m below the sea surface at M3 (bottom depth 970 m), ~180 m at M6 (bottom depth 790 m), and ~ 180 m at M4 (bottom depth 1720 m) (Table 1), meaning that backscatter strength data were available only from the surface down to the ADCP installation depths of 180–190 m. At these offshore sites, the vertical structure of the first mode showed no clear nodal points like at M1 and M5, and there were no large vertical phase differences. This suggests that zooplankton were diving deeper than the ADCP installation depths of 180–190 m during the daytime as part of their DVM. Based on this deep-diving behavior, the DVM observed at these sites is presumed to be driven by krill (Mauchline and Fisher, 1969). Based on previous reports and the observed temperature range along the eastern Sakhalin coast, candidates of the dominant krill species exhibiting DVM are *Euphausia pacifica*, *Thysanoessa longipes* and *T. raschii* (Tomiyama et al., 2017; Mauchline, 1980). Although ecological information on krill in the Sea of Okhotsk—particularly regarding their life cycles and seasonal abundance—has been reported (e.g., Tomiyama et al., 2017), there is limited information on their DVM behavior. This study is the first to quantify the intensity of DVM throughout an entire year and to examine its regional variability.

We next discuss the results off the east Sakhalin coast. As seen in Fig. 10, from spring through summer, chlorophyll-a concentrations are relatively high along the Sakhalin coastal area and relatively low in offshore areas. This spatial pattern is likely attributable to greater inputs of micronutrients such as iron in the shelf regions from resuspended sediments and/or coastal-origin sea ice (Nishioka et al., 2014; Kuga et al., 2023; 2024). During winter sea-ice season, our ADCP backscatter data suggest that zooplankton activity is possibly more vigorous in the offshore region than over the shelf region. If this is the case, it demonstrates contrasting dynamics between the two regions across summer and winter.

One possible explanation for the winter differences between these regions is differences in the dominant zooplankton species and their characteristics. The dominant zooplankton in the offshore regions are presumed to be krill, based on their deep-diving DVM, and are considered to maintain DVM activity even in winter. On the other hand, copepods are thought to dominate on the shelf regions, and they are presumed not to perform prominent DVM in winter. Another factor could be sea-ice thickness. Coastal shelf regions tend to have thicker,

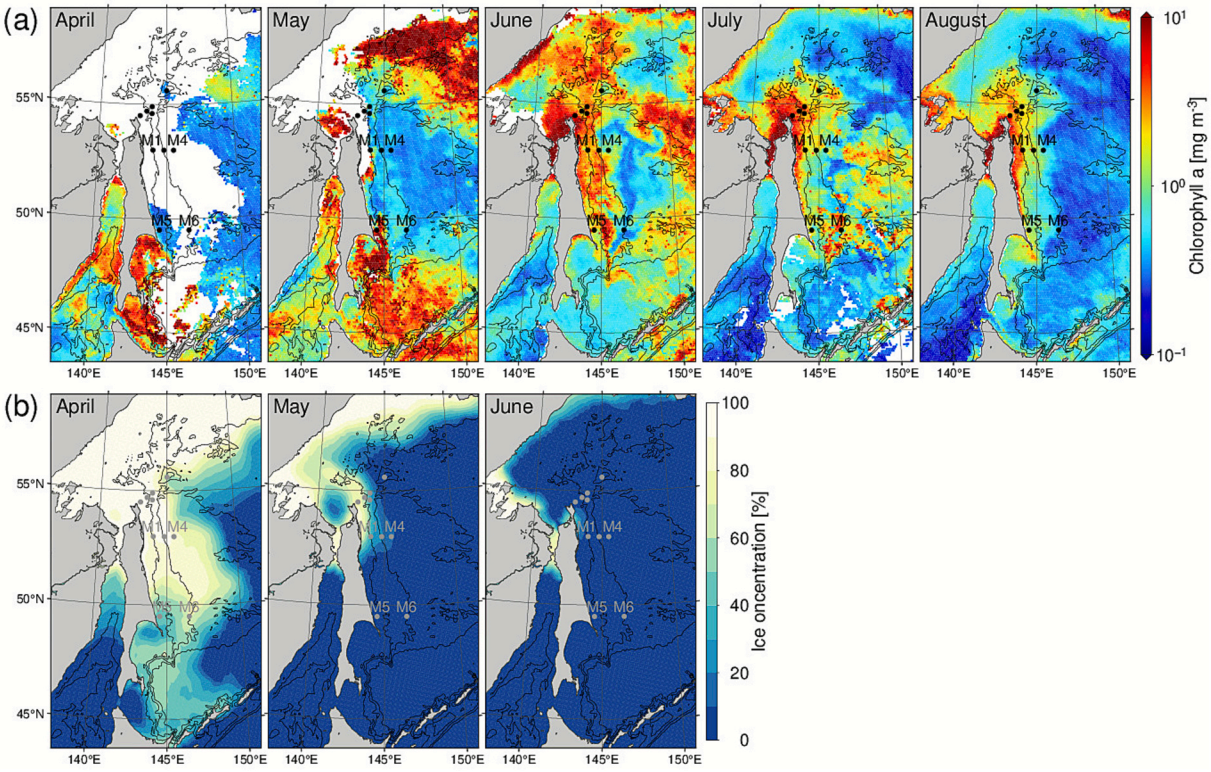

Fig. 10. Monthly maps of (a) MODIS-Aqua chlorophyll-a concentration from April to August 1998 and (b) sea ice concentration from April to June 1998. Bathymetric contours of 200, 1000, and 2000 m are indicated by solid lines.

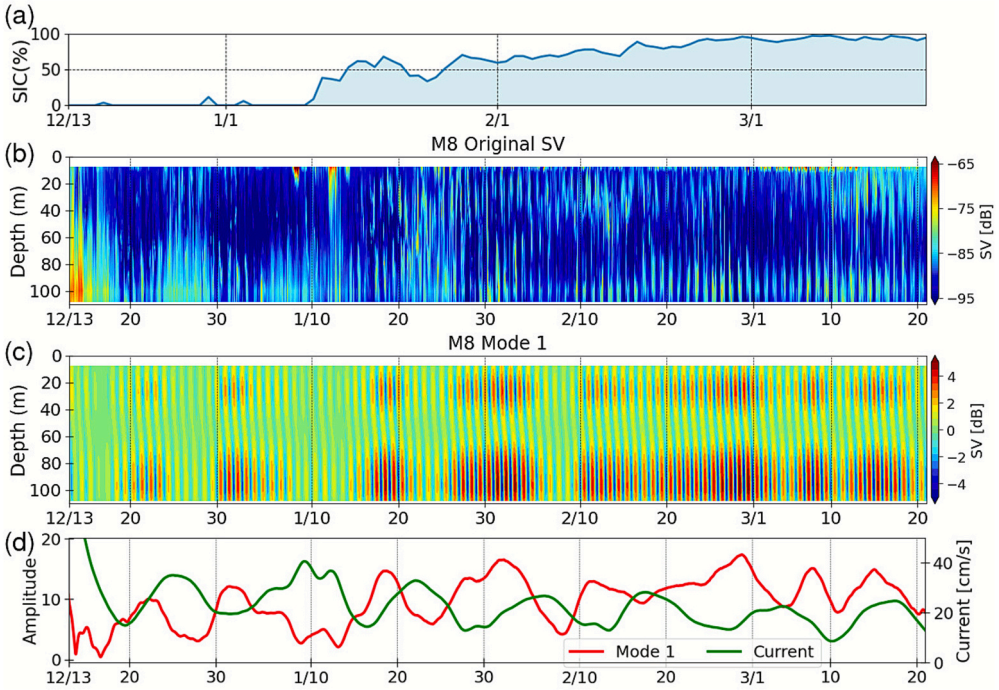

Fig. 11. Time series at M8 from December 1999 to March 2000 of (a) sea ice concentration, (b) vertical profiles of original volume backscatter strength (SV), (c) reconstructed first CEOF mode, and (d) temporal amplitude of the first mode score (red) and the absolute velocity with a fortnightly bandpass filter at the near-bottom bin (green).

more developed sea ice than offshore regions (Nihashi et al., 2018; Honda et al., 2024), which greatly reduces light penetration and may suppress DVM activity. Additionally, thick sea ice promotes the development of ice algae, and if copepods feeding on ice-associated algae (Yan et al., 2020) are the dominant species, prominent DVM behavior would not be expected.

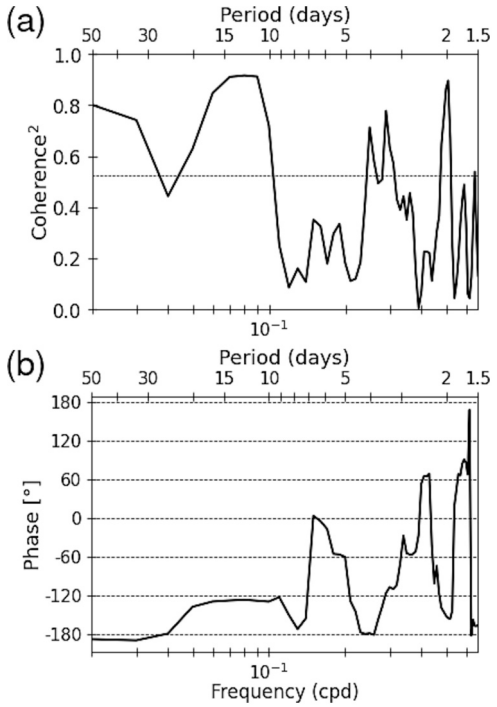

Fig. 12. (a) Squared coherence and (b) phase of the cross-spectra between the first CEOF mode score and absolute near-bottom current velocity at M8. A positive phase indicates that the first CEOF mode leads the bottom current. The 95% confidence level is shown in (a).

5. Application to the region of the northern Sakhalin shelf with strong tidal currents

The northern Sakhalin shelf region, similar to M15 at Kashevarova Bank, is an area with extremely strong tidal currents. According to the dispersion relation characteristics of coastal-trapped waves, diurnal coastal-trapped waves can exist only on the shelf north of 51–52°N in northern Sakhalin, generating strong tidal currents (Ohshima et al., 2002; Ono et al., 2008; 2010). Due to the strength of these tidal currents, sediment resuspension has been reported at M8 and M9 during periods of strong currents when the East Sakhalin Current overlaps with the tidal currents (Ito et al., 2017). Fig. 11 presents the original backscatter strength and CEOF analysis results at M8. When the TRBM (trawl-resistant bottom mount) installing an ADCP was deployed at M8 in September 1999, it was unintentionally installed upside down on the seafloor, preventing data acquisition until mid-December 1999. Fortunately, during a strong current event, the TRBM was restored to its normal orientation, allowing data collection from mid-December 1999 to March 2000. The CEOF analysis over this three-month period shows that the first CEOF mode has large spatial amplitudes in the surface and near-bottom layers, with a phase difference of 180 degrees, clearly representing DVM. The time series of the first mode reveals a semi-monthly periodicity. Fig. 11d represents the time series of the first mode score and the absolute velocity with a fortnightly bandpass filter at the near-bottom bin, showing a clear inverse relationship—when the current velocity increases, the first mode amplitude decreases. Fig. 12 presents the cross-spectrum of the first mode score and the absolute velocity, showing high coherence at fortnightly periods. The phase difference suggests that the DVM represented by the first CEOF mode weakens approximately two days after peak tidal currents during spring tides. Similar results (not shown) were obtained at M9, which is located slightly closer to shore than M8.

We also conducted similar CEOF analysis for M7, located on the continental slope. Due to strong currents, the ADCP at M7 was displaced southward twice, resulting in changes in its position and depth (Fig. 1; Table 1). Accordingly, the analysis was conducted separately for three different periods. Examination of the first CEOF mode across these periods shows that, although the ADCP depth range varied significantly, the node consistently appeared around 150 m below the surface, and the phase behavior remained largely unchanged. These findings might imply that the CEOF analysis captures the DVM of a common zooplankton species across the different positions and periods. Fig. 13b shows the time series of the first and second mode scores and the absolute velocity with a fortnightly bandpass filter at the lowest ADCP bin, again indicating an inverse relationship—stronger currents correspond to a lower amplitude in the first mode. Fig. 14 presents the cross-spectrum of the first mode score and the absolute velocity for each of the three periods (three different positions). As in the case of M8, high coherence is observed at fortnightly periods, with a phase difference of 180 degrees. These results indicate that DVM, as represented by the first CEOF mode, is at its weakest during spring tides, when tidal currents are strongest.

Consistent weakening of DVM under strong tidal currents was observed at five locations (M8, M9, and three positions of the drifting M7), suggesting that this marked correlation is not due to local advection but reflects a region-wide phenomenon across the strong tidal current area. Regarding the relationship between zooplankton and tidal currents, several studies have reported that surface swarming tends to occur only during spring tides (e.g., Brown et al., 1980; Gómez-Gutiérrez and Robinson, 2006). Although the mechanisms behind such swarming have not been well understood, one hypothesis is that it arises passively due to convergence and upwelling induced by strong tidal currents. If surface swarming is induced also in this region by strong tidal currents, the resulting decrease in zooplankton abundance within the subsurface layer during spring tides could account for the observed reduction in

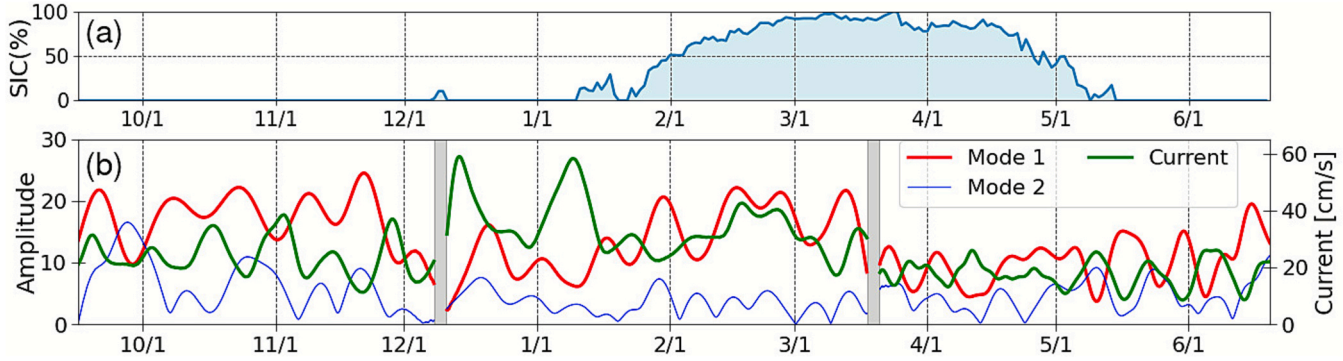

Fig. 13. Time series at M7 from September 1999 to June 2000 of (a) sea ice concentration, (b) temporal amplitude of the first (red) and second (blue) CEOF mode scores of SV and the absolute velocity with a fortnightly bandpass filter at the deepest bin (green). The CEOF analysis was conducted separately for three periods, September–November 1998, December 1998–March 1999, and March–June 1999, as indicated by gray bars.

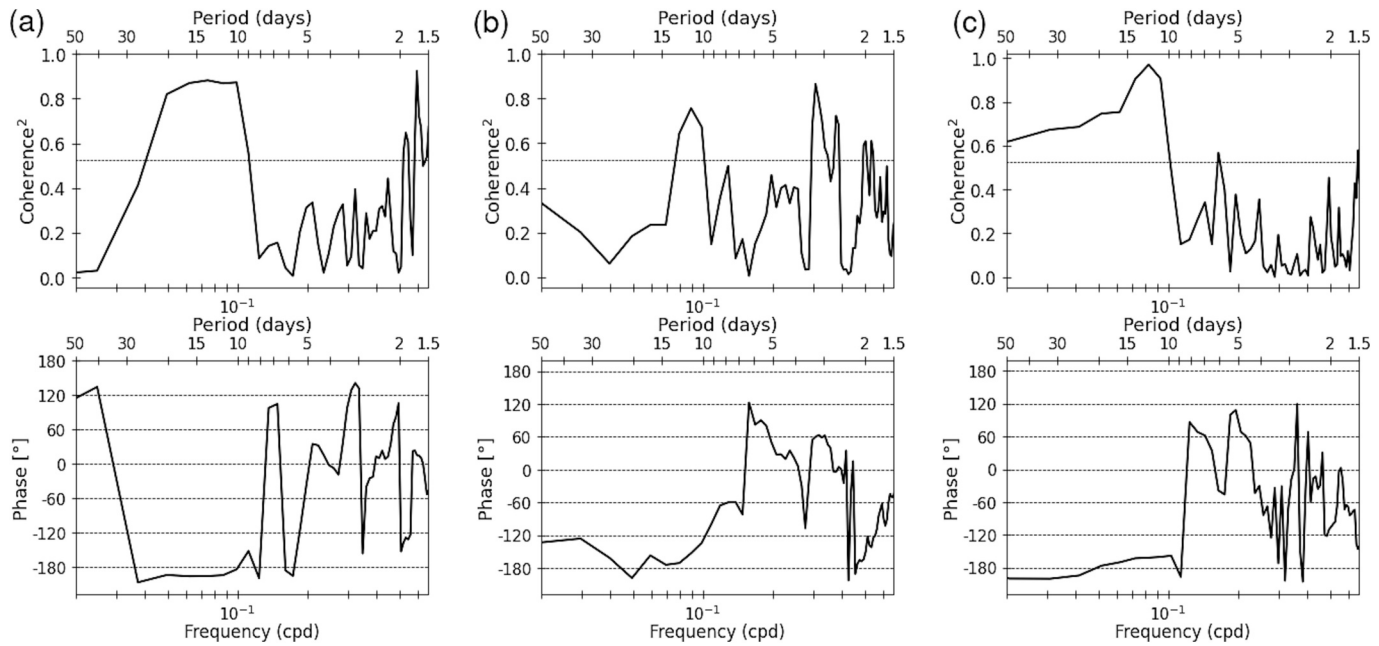

Fig. 14. (Upper panels) Squared coherence and (lower panels) phase of the cross-spectra between the first CEOF mode score and absolute velocity at the deepest bin at M7 for (a) September–November 1998, (b) December 1998–March 1999, and (c) March–June 1999. A positive phase indicates that the first CEOF mode leads the current speed. The 95% confidence level is shown in the upper panels.

DVM intensity.

6. Concluding remarks

Acoustic Doppler Current Profilers (ADCPs) provide not only velocity profiles but also backscatter strength data, which can be used to detect suspended materials in the water column. Specific suspended materials detectable include zooplankton associated with diel vertical migration (DVM), sediment resuspension, and underwater frazil ice. However, no established method exists to reliably distinguish among these components.

In this study, we developed a novel approach to detect and distinguish between zooplankton DVM and sediment resuspension linked to tidal current variability by applying CEOF (Complex Empirical Orthogonal Function) analysis to 24-hour bandpass-filtered ADCP backscatter data. DVM is extracted as a mode characterized by large amplitudes near the surface at nighttime and near the seafloor or lower layers during the daytime. In contrast, sediment resuspension is extracted as a mode with little phase difference across depths and larger amplitudes closer to the bottom. Although both signals share a 24-hour periodicity, CEOF analysis allows clear separation by resolving phase differences. Notably, the temporal CEOF mode scores provide objective scalar indices of the intensity of each phenomenon, enabling quantitative comparisons with environmental factors such as sea ice and tidal currents.

We applied this approach to year-round ADCP backscatter strength data from nine sites in the western Okhotsk Sea. The analysis successfully quantified DVM and revealed its seasonal and regional differences. At most sites, DVM activity is represented by the first CEOF mode and tended to intensify immediately after sea ice melt. As noted in previous studies, sea ice melt enhances stratification and releases iron, triggering phytoplankton blooms, which subsequently feed zooplankton. DVM activation, represented by the first mode, begins earlier in the south. This is because sea ice melt occurs earlier in southern regions. During spring and summer, the shelf regions exhibit much higher chlorophyll concentrations than the offshore basin regions (Fig. 10), indicating more active biological productivity over the shelf regions. However, temporal variations of the first mode revealed that during the winter sea-ice season, DVM significantly weakens over the shelf regions but persists in the offshore regions. This contrasting seasonal behavior between shelf and offshore regions likely reflects differences in the dominant zooplankton species and their traits. According to the spatial structure of the first CEOF mode, offshore DVM reaches depths exceeding ~ 200 m. Thus, this DVM is likely associated with krill (euphausiids), which are thought to continue DVM even during winter. In contrast, the shelf regions, covered by thicker sea ice, are likely dominated by copepods that may feed on ice algae adhering to the ice underside, with little or no DVM activity.

Furthermore, the quantitative assessment of DVM revealed, through spectral analysis, a clear relationship with tidal currents. In the northwestern Okhotsk Sea, where tidal currents are strong, DVM activity, represented by the first CEOF mode, consistently reduces during spring tides. At Kashevarov Bank, the first mode represents sediment resuspension, and the second mode captures DVM. Spectral analysis showed that the first CEOF mode (sediment resuspension) at Kashevarov Bank is strongly correlated with tidal currents, with sediment resuspension intensifying ~ 1–1.5 days after peak tidal current velocities.

Although this study applied CEOF analysis to the entire observation period for all sites, shorter-term analyses may be more appropriate when DVM behavior changes seasonally. For example, at site M3, the daytime migration depth of DVM varied seasonally, suggesting that monthly CEOF analyses could help resolve the structural changes in DVM. Alternatively, as shown in Fig. 3 and used in previous studies, constructing 24-hour composites over specific periods can also be effective. It is noted that the CEOF approach is not universally effective and should be selected carefully according to the specific context. Given the vast quantity of unused ADCP backscatter (SV) data worldwide, we anticipate that the application of generalized methods such as the one proposed here will help unlock the potential of these dormant datasets.

CRediT authorship contribution statement

Kay I. Ohshima: Writing – review & editing, Writing – original draft, Visualization, Validation, Supervision, Resources, Project administration, Methodology, Investigation, Funding acquisition, Formal analysis, Data curation, Conceptualization. **Mamoru Ohshima:** Visualization,

Software, Methodology, Investigation, Formal analysis. **Masato Ito:** Formal analysis, Data curation. **Kazuki Nakata:** Visualization, Software, Methodology, Formal analysis. **Mizuki Kuga:** Visualization, Software, Data curation. **Kohei Matsuno:** Validation, Supervision. **Atsushi Yamaguchi:** Writing – original draft, Validation, Supervision.

Declaration of competing interest

The authors declare that they have no known competing financial interests or personal relationships that could have appeared to influence the work reported in this paper.

Acknowledgments

This work was supported by Grants-in-Aids for Scientific Research of the Ministry of Education, Culture, Sports, Science, and Technology in Japan, 20H05707 (to K.I.O.), 20K20933 (to K.I.O. and M.I.), and 25H00002 (to K.I.O.). The mooring data were obtained under the Joint Japanese-Russian-U.S. study of the Sea of Okhotsk, supported by the fund from the Core Research for Evolutional Science and Technology (representative: M. Wakatsuchi), Japanese Science and Technology Corporation, cooperating with Y. Fukamachi and G. Mizuta.

Appendix

We performed Complex Empirical Orthogonal Function (CEOF) analysis on the time series of volume backscatter strength (SV) obtained at m depth bins. First, for each bin, we calculated the anomaly time series by subtracting the long-term mean over the full observation period. A strong band-pass filter centered at 24h was then applied to each bin. For the M5 mooring, we used a filter with cutoff periods of 23h and 25h. The filtered data were subsequently multiplied by a Hamming window. Next, each time series was transformed using the Hilbert transformation, yielding complex-valued time series with n time samples for each of the m bins. These m sets of complex time series were arranged into an $n \times m$ matrix, with rows representing time and columns representing depth bins. From this matrix, we computed the covariance matrix C (a Hermitian matrix). The eigenvalues (real) and eigenvectors (complex) of C correspond to the variance contributions and mode structures of the CEOF decomposition, respectively.

In the Supplementary material, we provide the Python codes implementing the above procedure, as well as the following additional scripts: (1) Plotting the raw SV vertical profile time series (Fig. 4a), (2) Calculating the contribution rates of each CEOF mode (eigenvalue), (3) Plotting the time series of CEOF mode scores and phases (Fig. 4c), (4) Plotting the spatial amplitude distribution of each CEOF mode (Fig. 4e), (5) Plotting the spatial phase structure of each CEOF mode (Fig. 4f), (6) Reconstructing and plotting each CEOF mode as a time series (Fig. 4d).

Appendix A. Supplementary data

Supplementary data to this article can be found online at https://doi.org/10.1016/j.pocean.2025.103630.

Data availability

Sea-ice concentration data from SSM/I are provided by the National Snow and Ice Data Center (https://nsidc.org/data/nsidc-0079/versions/4). Chlorophyll-a concentration data from the SeaWiFS are provided by NASA's Ocean Biology Processing Group (https://oceandata.sci.gsfc.nasa.gov/l3/).

References

Arima, D., Yamaguchi, A., Nobetsu, T., Imai, I., 2016. Usefulness of deep-ocean water pumping for the seasonal monitoring of mesozooplankton. Reg. Stud. Mar. Sci. 3, 18–24. https://doi.org/10.1016/j.rsma.2015.06.001.

Berge, J., Daase, M., Renaud, P.E., Ambrose Jr, W.G., Darnis, G., Last, K.S., Callesen, T. A., 2015. Unexpected levels of biological activity during the polar night offer new perspectives on a warming Arctic. Curr. Biol. 25, 2555–2561. https://doi.org/10.1016/j.cub.2015.08.024.

Brown, R.G.B., Barker, S.P., Gaskin, D.E., 1980. Daytime surface swarming by *Meganyctiphanes norvegica* (M.Sars) (Crustacea, Euphausiacea) off Brier Island, Bay of Fundy. Can. J. Zool. 58, 2285–2291. https://doi.org/10.1139/z79-297.

Cohen, J.H., Berge, J., Moline, M.A., Sørensen, A.J., Last, K., Falk-Petersen, S., Johnsen, G., 2015. Is ambient light during the high Arctic polar night sufficient to act as a visual cue for zooplankton? PLoS One 10, e0126247. https://doi.org/10.1371/journal.pone.0126247.

Comiso, J.C., 1995. SSM/I Sea Ice Concentrations Using the Bootstrap Algorithm. National Aeronautics and Space Administration Reference publication 1380, 49.

Deines, K.L., 1999. Backscatter estimation using Broadband acoustic Doppler current profilers. In: Proceedings of the IEEE Sixth Working Conference on Current Measurement (Cat. No.99CH36331), San Diego, CA, pp.249–253. DOI: 10.1109/CCM.1999.755249.

Dmitrenko, I.A., Petrusevich, V., Darnis, G., Kirillov, S.A., Komarov, A.S., Ehn, J.K., Forest, A., Fortier, L., Rysgaard, S., Barber, D.G., 2020. Sea-ice and water dynamics and moonlight impact the acoustic backscatter diurnal signal over the eastern Beaufort Sea continental slope. Ocean Sci. 16, 1261–1283. https://doi.org/10.5194/os-16-1261-2020.

Dmitrenko, I.A., Petrusevich, P., A., Kosobokova, K., Bouchard, C., Geoffroy, M., Komarov, A. S., Babb, D. G., Kirillov, S. A., Barber, D. G., 2024. Contrasting two major Arctic coastal polynyas: the role of sea ice in driving diel vertical migrations of zooplankton in the Laptev and Beaufort seas. Ocean Sci. 20, 1677–1705. https://doi.org/10.5194/os-20-1677-2024.

Downing, A., Thorne, P.D., Vincent, C.E., 1995. Backscattering from a suspension in the near field of a piston transducer. J. Acoust. Soc. Am. 97 (3), 1614–1620. https://doi.org/10.1121/1.412100.

Enright, J.T., 1977. Copepods in a hurry: Sustained high-speed upward migration. Limnol. Oceanogr. 22, 118–125.

Flores, H., Veyssière, G., Castellani, G., et al., 2023. Sea-ice decline could keep zooplankton deeper for longer. Nat. Clim. Chang. 13, 1122–1130. https://doi.org/10.1038/s41558-023-01779-1.

Gómez-Gutiérrez, J., Robinson, C.J., 2006. Tidal current transport of epibenthic swarms of the euphausiid *Nyctiphanes simplex* in a shallow, subtropical bay on Baja California peninsula, México. Mar. Ecol. Prog. Ser. 320, 215–231. https://doi.org/10.3354/meps320215.

Honda, M., Ohshima, K.I., Mensah, V., Nishioka, J., Sato, M., Riser, S.C., 2024. Sea ice-melt amount estimated from spring hydrography in the Sea of Okhotsk: spatial and interannual variabilities. J. Oceanogr. 80, 273–290. https://doi.org/10.1007/s10872-024-00721-z.

Ito, M., Ohshima, K.I., Fukamachi, Y., Mizuta, G., Kusumoto, Y., Nishioka, J., 2017. Observations of frazil ice formation and upward sediment transport in the Sea of Okhotsk: A possible mechanism of iron supply to sea ice. J. Geophys. Res. Oceans 122, 788–802. https://doi.org/10.1002/2016JC012198.

Ito, M., Fukamachi, Y., Ohshima, K.I., Shirasawa, K., 2020. Observational evidence of supercooling and frazil ice formation throughout the water column in a coastal polynya in the Sea of Okhotsk. Cont. Shelf Res. 196, 104072. https://doi.org/10.1016/j.csr.2020.104072.

Ito, M., Ohshima, K.I., Fukamachi, Y., Mizuta, G., Kusumoto, Y., Kikuchi, T., 2021. Underwater frazil ice and its suspension depth detected from ADCP backscatter data around sea ice edge in the Sea of Okhotsk. Cold Reg. Sci. Technol. 192, 103382. https://doi.org/10.1016/j.coldregions.2021.103382.

Itoh, H., Nishioka, J., Tsuda, A., 2014. Community structure of mesozooplankton in the western part of the Sea of Okhotsk in summer. Prog. Oceanogr. 126, 224–232. https://doi.org/10.1016/j.pocean.2014.05.006.

Kanna, N., Toyota, T., Nishioka, J., 2014. Iron and macro-nutrient concentrations in sea ice and their impact on the nutritional status of surface waters in the southern Okhotsk Sea. Prog. Oceanogr. 126, 44–57. https://doi.org/10.1016/j.pocean.2014.04.012.

Kanna, N., Sibano, Y., Toyota, T., Nishioka, J., 2018. Winter iron supply processes fueling spring phytoplankton growth in a sub-polar marginal sea, the Sea of Okhotsk: Importance of sea ice and the East Sakhalin Current. Mar. Chem. 206, 109–120. https://doi.org/10.1016/j.marchem.2018.08.006.

Kishi, S., Ohshima, K.I., Nishioka, J., Isshiki, N., Nihashi, S., Riser, S.C., 2021. The prominent spring bloom and its relation to sea ice melt in the Sea of Okhotsk, revealed by profiling floats. Geophys. Res. Lett. 48, e2020GL091394. https://doi.org/10.1029/2020GL091394.

Kojima, D., Hamao, Y., Amei, K., Fukai, Y., Matsuno, K., Mitani, Y., Yamaguchi, A., 2022. Vertical distribution, standing stocks, and taxonomic accounts of the entire plankton community, and the estimation of vertical material flux via faecal pellets in the southern Okhotsk Sea. Deep-Sea Res. I 185, 103771. https://doi.org/10.1016/j.dsr.2022.103771.

Kowalik, Z., Polyakov, I., 1998. Tides in the Sea of Okhotsk. J. Phys. Oceanogr. 28, 1389–1409. https://doi.org/10.1175/1520-0485(1998)028.1389:TITSOO.2.0.CO;2.

Kuga, M., Ohshima, K.I., Kimura, N., Nakata, K., Fukamachi, Y., 2023. Particle-tracking experiments of coastal-origin sea ice that could induce high biological productivity in the Sea of Okhotsk. J. Oceanogr. 79, 145–159. https://doi.org/10.1007/s10872-022-00670-5.

Kuga, M., Ohshima, K.I., Kishi, S., Kimura, N., Toyota, T., Nishioka, J., 2024. Backward-tracking simulations of sea ice in the Sea of Okhotsk toward understanding of material transport through sea ice. J. Oceanogr. 80, 59–70. https://doi.org/10.1007/s10872-023-00706-4.

Martin, S., Polyakov, I., Markus, T., Drucker, R., 2004. Okhotsk Sea Kashevarov Bank polynya: its dependence on diurnal and fortnightly tides and its initial formation. J. Geophys. Res. 109, C09S04. https://doi.org/10.1029/2003JC002215.

Mauchline, J., Fisher, L.R., 1969. The biology of euphausiids. Adv. Mar. Biol. 7, 1–454.

Mauchline, J., 1980. The biology of mysids and euphausiids. Adv. Mar. Biol. 18, 1–677.

Mauchline, J., 1998. The biology of calanoid copepods. Adv. Mar. Biol. 33, 1–710.

Mizuta, G., Fukamachi, Y., Ohshima, K.I., Wakatsuchi, M., 2003. Structure and seasonal variability of the East Sakhalin Current. J. Phys. Oceanogr. 33, 2430–2445. https://doi.org/10.1175/1520-0485(2003)033.2430:SASVOT.2.0.CO;2.

Moroshkin, K.V., 1966. Water masses of the Sea of Okhotsk. U.S. Dept. of Commerce Joint Publication Research Service 43942, 98 pp.

Nakamura, T., Awaji, T., Hatayama, T., Akitomo, K., Takizawa, T., 2000. Tidal exchange through the Kuril Straits. J. Phys. Oceanogr. 30, 1622–1644. https://doi.org/10.1175/1520-0485(2000)030.1622:TETTKS.2.0.CO;2.

Niebauer, H.J., Alexander, V., Henrichs, S., 1990. Physical and biological oceanographic interaction in the spring bloom at the Bering Sea marginal ice edge zone. J. Geophys. Res. 95, C12. https://doi.org/10.1029/JC095iC12p22229.

Nihashi, S., Ohshima, K.I., Tamura, T., Fukamachi, Y., Saitoh, S., 2009. Thickness and production of sea ice in the Okhotsk Sea coastal polynyas from AMSR-E. J. Geophys. Res. 114, C10025. https://doi.org/10.1029/2008JC005222.

Nihashi, S., Ohshima, K.I., Kimura, N., 2012. Creation of a heat and salt flux dataset associated with sea ice production and melting in the Sea of Okhotsk. J. Clim. 25, 2261–2278. https://doi.org/10.1175/JCLI-D-11-00022.1.

Nihashi, S., Kurtz, N.T., Markus, T., Ohshima, K.I., Tateyama, K., Toyota, T., 2018. Estimation of sea-ice thickness and volume in the Sea of Okhotsk based on ICESat data. Ann. Glaciol. 59 (76pt2), 101–111. https://doi.org/10.1017/aog.2018.8.

Nishioka, J., Nakatsuka, T., Ono, K., Volkov, Y.N., Scherbinin, A., Shiraiwa, T., 2014. Quantitative evaluation of iron transport processes in the Sea of Okhotsk. Progress in Oceanography 126, 180–193. https://doi.org/10.1016/j.pocean.2014.04.011.

Ohshima, K.I., Wakatsuchi, M., Fukamachi, Y., Mizuta, G., 2002. Near-surface circulation and tidal currents of the Okhotsk Sea observed with satellite-tracked drifters. J. Geophys. Res. 107, 3195. https://doi.org/10.1029/2001JC001005.

Ohshima, K.I., Nihashi, S., Iwamoto, K., 2016. Global view of sea-ice production in polynyas and its linkage to dense/bottom water formation. Geosci. Lett. 3, 13. https://doi.org/10.1186/s40562-016-0045-4.

Ono, J., Ohshima, K.I., Mizuta, G., Fukamachi, Y., Wakatsuchi, M., 2006. Amplification of diurnal tides over Kashevarov Bank in the Sea of Okhotsk and its impact on water mixing and sea ice. Deep Sea Res., Part I 53, 409–424. https://doi.org/10.1016/j.dsr.2005.12.002.

Ono, J., Ohshima, K.I., Mizuta, G., Fukamachi, Y., Wakatsuchi, M., 2008. Diurnal coastal-trapped waves on the eastern shelf of Sakhalin in the Sea of Okhotsk and their modification by sea ice. Cont. Shelf Res. 28, 697–709. https://doi.org/10.1016/j.csr.2007.11.003.

Ono, J., Ohshima, K.I., 2010. Numerical model studies on the generation and dissipation of the diurnal coastal-trapped waves over the Sakhalin shelf in the Sea of Okhotsk. Cont. Shelf Res. 30, 588–597. https://doi.org/10.1016/j.csr.2009.12.004.

Petrusevich, V., Dmitrenko, I.A., Kirillov, S.A., Rysgaard, S., Falk-Petersen, S., Barber, D. G., Ehn, J.K., 2016. Wintertime water dynamics and moonlight disruption of the acoustic backscatter diurnal signal in an ice-covered Northeast Greenland fjord. J. Geophys. Res. 121, 4804–4818. https://doi.org/10.1002/2016JC011742.

Petrusevich, V.Y., Dmitrenko, I.A., Niemi, A., Kirillov, S.A., Kamula, C.M., Kuzyk, Z.Z.A., Barber, D.G., Ehn, J.K., 2020. Impact of tidal dynamics on diel vertical migration of zooplankton in Hudson Bay. Ocean Sci. 16, 337–353. https://doi.org/10.5194/os-16-337-2020.

Pinchuk, A., Paul, A.J., 2000. Zooplankton of the Okhotsk Sea: A Review of Russian Studies. University of Alaska Sea Grant, Anchorage.

Rabinovich, A.B., Zhukov, A.E., 1984. Tidal oscillations on the shelf of Sakhalin Island. Oceanology 24, 184–189.

Rogachev, K.A., Carmack, E.C., Salomatin, A.S., Alexanina, M.G., 2001. Lunar fortnightly modulation of tidal mixing near Kashevarov Bank, Sea of Okhotsk, and its impacts on biota and sea ice. Prog. Oceanogr. 49, 373–390. https://doi.org/10.1016/S0079-6611(01)00040-1.

Sakamoto, T., Ikehara, M., Aoki, K., Iijima, K., Kimura, N., Nakatsuka, T., Wakatsuchi, M., 2005. Ice-rafted debris (IRD)-based sea-ice expansion events during the past 100kyrs in the Okhotsk Sea, Deep-Sea Res. II 52, 2275–2301. https://doi.org/10.1016/j.dsr2.2005.08.007.

Simizu, D., Ohshima, K.I., 2006. A model simulation on the circulation in the Sea of Okhotsk and the East Sakhalin Current. J. Geophys. Res. 111, C05016. https://doi.org/10.1029/2005JC002980.

Simizu, D., Ohshima, K.I., Ono, J., Fukamachi, Y., Mizuta, G., 2014. What drives the southward drift of sea ice in the Sea of Okhotsk? Prog. Oceanogr. 126, 33–43. https://doi.org/10.1016/j.pocean.2014.05.013.

Sorokin, Y.I., Sorokin, P.Y., 1999. Production in the Sea of Okhotsk. J. Plankton Res. 21, 201–230. https://doi.org/10.1093/plankt/21.2.201.

Takahashi, K., Kuwata, A., Sugisaki, H., Uchikawa, K., Saito, H., 2009. Downward carbon transport by diel vertical migration of the copepods *Metridia pacifica* and *Metridia okhotensis* in the Oyashio region of the western subarctic Pacific Ocean. Deep-Sea Research I 56, 1777–1791. https://doi.org/10.1016/j.dsr.2009.06.005.

Tomiyama, K., Matsuno, K., Abe, Y., Shimada, H., Yamaguchi, A., 2017. Inter-oceanic differences in macrozooplankton biomass and community structure in four regions around Hokkaido Island, Japan: consequences for marine ecosystem structure. Bull. Fish. Sci. Hokkaido Univ. 67 (2), 25–34. https://doi.org/10.14943/bull.fish.67.2.25.

Tsuda, A., Saito, H., Kasai, H., Nishioka, J., Nakatsuka, T., 2015. Vertical segregation and population structure of ontogenetically migrating copepods Neocalanus cristatus, N. flemingeri, N. plumchrus, and Eucalanus bungii during the ice-free season in the Sea of Okhotsk. J. Oceanogr. 71, 271–285. https://doi.org/10.1007/s10872-015-0287-3.

Vinogradov, M.E., 1954. Diurnal vertical migrations of zooplankton in the far-eastern seas. Tr. Inst. Okeanol. Akad. Nauk. SSSR 8, 164–199. In Russian.

Wong, C.K., 1988. The swimming behavior of the copepod *Metridia pacifica*. J. Plankton Res. 10, 1285–1290. https://doi.org/10.1093/plankt/10.6.1285.

Yamaguchi, A., 2015. Inter-oceanic comparison of planktonic copepod ecology (vertical distribution, abundance, community structure, population structure and body size) between the Okhotsk Sea and Oyashio region in autumn. J. Nat. Hist. https://doi.org/10.1080/00222933.2015.1022616.

Yan, D., Yoshida, K., Nishioka, J., Ito, M., Toyota, T., Suzuki, K., 2020. Response to sea ice melt indicates high seeding potential of the ice diatom *Thalassiosira* to spring phytoplankton blooms: A laboratory study on an ice algal community from the Sea of Okhotsk. Front. Mar. Sci. 7, 613. https://doi.org/10.3389/fmars.2020.00613.